# Oxygen Atoms on Cu(100) Formed at 100 K, Active for CO Oxidation and Water−Hydrogen Abstraction, Characterized by HREELS and TPD

**Tsuyoshi Sueyoshi, Takehiko Sasaki, and Yasuhiro Iwasawa***

*Department of Chemistry, Graduate School of Science, The University of Tokyo, Hongo, Bunkyo-ku, Tokyo 113, Japan*

*Received: February 7, 1997; In Final Form: April 7, 1997*[⊗]

The reactivity of oxygen adatoms formed by dissociative adsorption of $O_2$ on Cu(100) at 100 K for CO oxidation and hydrogen abstraction from water was investigated by means of HREELS and TPD in comparison with the reactivity of adsorbed oxygen in thermally stable phases. The oxygen adatoms formed on the Cu(100) surface by exposure to $O_2$ at 100 K, designated as as-exposed oxygen, were found to be reactive with coadsorbed CO to yield a $CO_2$ desorption peak at 125 K in TPD. The as-exposed oxygen atoms are suggested to be more active for CO oxidation than the oxygen atoms prepared above room temperature on Pt and Pd, which are the most active metals for CO oxidation. On annealing the oxygen−as-exposed surfaces to 300 K, a change in the loss feature of $\nu$(Cu−O) was observed, which was indicative of formations of a pseudo c(2×2)-O phase with O(a) in 4-fold hollow sites and a ($\sqrt{2}\times2\sqrt{2}$)*R*45°-O phase comprised of −Cu−O− chains grown along the [001] direction. On these two phases, $CO_2$ formation in TPD was suppressed by 1 order of magnitude. Isolated oxygen atoms in the as-exposed surface are responsible for the high reactivity for CO oxidation. Hydrogen abstraction from water was also examined as a probe reaction for oxygen adatoms on different phases. The as-exposed surface and the pseudo c(2×2)-O phase were found to be reactive and OH(a) was detected by means of HREELS after subsequent exposure to water at 100 K. In contrast, the ($\sqrt{2}\times2\sqrt{2}$)-*R*45°-O phase in which oxygen atoms were incorporated into −Cu−O− chains was inert.

## 1. Introduction

The reactivity of adsorbed oxygen on metal surfaces has received considerable interest in relation to heterogeneous catalysis. In particular, CO oxidation on Pt, Pd, and Rh has been studied extensively because of the importance of the fundamental and practical aspects.[1,2] In contrast to the high reactivity of these metals, late transition metals like Cu are regarded to be much less reactive because stable oxide phases are easily produced due to their large oxygen affinity. In recent studies, however, oxygen atoms on metallic Cu surfaces were found to be reactive.[3−7] It was reported that CO oxidation proceeded on metallic Cu films at 473−623 K with a smaller activation energy than those for Pt and Pd.[3] We recently found that atomic oxygen on unreconstructed Cu(110) formed below 230 K was reactive for CO oxidation, and the reactivity was lost above 250 K, where oxygen atoms were incorporated into a Cu(110)-(2×1)-O phase comprised of −Cu−O− chains along the [001] direction.[4−7] The catalytic CO oxidation on Cu(110) in a mixture of CO and $O_2$ also continued to proceed at low temperatures until oxygen coverage increased to cover the surface with the produced −Cu−O− chains, which provides a definite self-poisoning phenomenon. Thus it may be valuable to examine the reactivity of adsorbed oxygen on other Cu metal surfaces for CO oxidation.

The reactivity of adsorbed oxygen for hydrogen abstraction from H-containing species such as $H_2O$, $NH_3$, and alcohols has also gained much attention in view of electrochemistry and catalysis.[8] Recent STM and Monte Carlo simulation studies revealed that the reactivity of oxygen adatoms was affected by microscopic changes in surface structures induced by oxygen adsorption.[9−12] For hydrogen abstraction from water on Cu(100), two different intermediate species were proposed: atomic oxygen formed at 300 K[13] and transient molecular oxygen.[14] Therefore, further investigation of reactive oxygen species for hydrogen abstraction on Cu(100) is necessary.

Oxygen adsorption on Cu(100) has been investigated using various methods such as LEED,[15,16] HREELS,[17,18] photoelectron diffraction,[19] SEXAFS,[20,21] NEXAFS,[20] STM,[16,22] and photoelectron spectroscopy.[23,24] Most of studies concentrated on adsorption above room temperature and revealed that the only structure with long-range order is the reconstructed ($\sqrt{2}\times2\sqrt{2}$)-*R*45°-O structure with a saturation coverage of 0.5 ML. In the ($\sqrt{2}\times2\sqrt{2}$)*R*45°-O phase, paired −Cu−O− chains grow along the [001] direction and every fourth row of Cu atoms along the [001] direction is removed.[16,22,25,26] In addition, the existence of a different phase without long-range order, designated as a pseudo c(2×2)-O phase, was verified below 0.34 ML.[18,19,21] A recent SEXAFS study concluded that atomic oxygen adsorbs in 4-fold hollow sites in the pseudo c(2×2)-O phase.[21] This model was consistent with a recent STM study.[26] The ($\sqrt{2}\times2\sqrt{2}$)*R*45°-O phase and the pseudo c(2×2)-O phase were characterized by different frequencies of $\nu$(Cu−O) at 290 and at 340 $cm^{-1}$, respectively, and the formation of the two phases was monitored at various coverage using HREELS.[17,18] In the HREELS studies, the pseudo c(2×2)-O phase was found to be predominant below 0.13 ML. The ($\sqrt{2}\times2\sqrt{2}$)*R*45° phase started to grow above 0.13 ML and coexisted with the pseudo c(2×2)-O phase up to 0.34 ML. Above 0.34 ML, all oxygen atoms were incorporated into the ($\sqrt{2}\times2\sqrt{2}$)*R*45°-O phase. The oxygen atoms in these phases were reduced at 473−623 K under exposure to $2.6\times10^{-4}$ to $1.3\times10^{-2}$ Pa of CO[27,28] and at 300 K under exposure to $1.2\times10^{3}$ Pa of CO.[29]

With regard to oxygen adsorption on Cu(100) below room temperature, both molecular and atomic oxygen species were detected after exposure to 500−1000 langmuirs at 100 K using photoelectron spectroscopy.[23,24] Molecular oxygen was also

* Corresponding author. Fax: +81-3-3814-2627. E-mail: iwasawa@chem.s.u-tokyo.ac.jp.

[⊗] Abstract published in *Advance ACS Abstracts,* May 15, 1997.

S1089-5647(97)00494-X CCC: $14.00 

found to be formed at 60 K and dissociate on annealing to 100 K.[20] In these studies, the oxygen adlayers formed at low temperatures were not investigated by HREELS. Furthermore, the reactivity of the atomic oxygen formed at 100 K has not been clarified well. The purpose of the present study is to characterize oxygen adlayers formed by exposure at 100 K, designated as as-exposed surfaces, by means of HREELS and to investigate differences in the reactivity of atomic oxygen among the as-exposed adlayer, the pseudo c(2×2)-O phase, and the $(\sqrt{2}\times2\sqrt{2})R45°$-O phase. In the present study, oxygen atoms in the as-exposed surface were found to be much more reactive for CO oxidation than those in the pseudo c(2×2)-O and $(\sqrt{2}\times2\sqrt{2})R45°$-O phases. For hydrogen abstraction from water, both the as-exposed surface and the pseudo c(2×2)-O phase were reactive, while the reactivity of oxygen atoms was lost in the $(\sqrt{2}\times2\sqrt{2})R45°$-O phase, where oxygen atoms are incorporated in −Cu−O− chains.

## 2. Experimental Section

All experiments were performed in an UHV chamber equipped with rearview LEED/AES optics, a quadrupole mass spectrometer, and a home-built HREELS spectrometer, as described elsewhere.[5] The mass spectrometer was enclosed in a glass cap with a hole of 6 mm diameter. The contribution except from a sample surface could be suppressed when the sample was placed in front of the hole at a distance of 2 cm.[5,6]

A Cu(100) sample with a purity of 5 N was purchased from MaTerial-Technologie and Kristalle GmbH (Jülich). The sample was suspended by a U-shaped Ta wire threading through two in-plane holes of the sample.[30] The sample temperature was measured by a thermocouple comprised of W−Re(5%) and W−Re(26%) spot-welded to the Ta wire in the vicinity of the sample. The sample was cooled down to 100 K by a liquid nitrogen reservoir installed in a sample holder and heated resistively to 1000 K at 2 K/s using a PID controller. All TPD spectra were measured at a heating rate of 2 K/s. The sample was cleaned by cycles of $Ar^+$ sputtering (0.5 keV, 7 $\mu$A/cm$^2$, 50 min) at 300 K and annealing at 700 K for 15 min. The sample cleanliness was checked by AES and LEED. Gases used in this study were introduced into the chamber by backfilling through variable leak valves.

The amount of desorbed CO was determined by integrating TPD peaks and was calibrated based on the saturation coverage of c(2×2)-CO structure (0.5 ML).[31−33] The amount of desorbed $CO_2$ was also determined by integrating TPD peaks and was calibrated by measuring a relative mass intensity ratio of $CO_2$ to CO in consideration of the relative sensitivity of $CO_2$ to CO for a B-A gauge[34] in a way similar to our previous studies.[5,6] The difference in pumping speed and conductance between CO and $CO_2$ was also taken into account in the estimation. Oxygen coverage on Cu(100) was estimated by means of AES based on the saturation coverage of $(\sqrt{2}\times2\sqrt{2})R45°$-O structure (0.5 ML).[18,21,22] The $(\sqrt{2}\times2\sqrt{2})R45°$-O phase with saturation coverage was prepared by exposing to 1200 langmuirs of oxygen at 500 K.[18]

## 3. Results

**3.1. Oxygen Adsorption on Cu(100).** Figure 1 shows HREEL spectra for oxygen adlayers on Cu(100). The feature of $\nu$(Cu−O) varied with oxygen coverage, exposing temperature, and annealing temperature. Change in the loss feature with increasing oxygen coverage above 300 K is shown in spectra i−iii. At 0.11 ML (i), a peak at 340 cm$^{-1}$ is assigned to $\nu$(Cu−O) of O(a) in the pseudo c(2×2)-O phase, where O(a) is located in a 4-fold hollow site.[18,21] At 0.26 ML (ii), a new peak

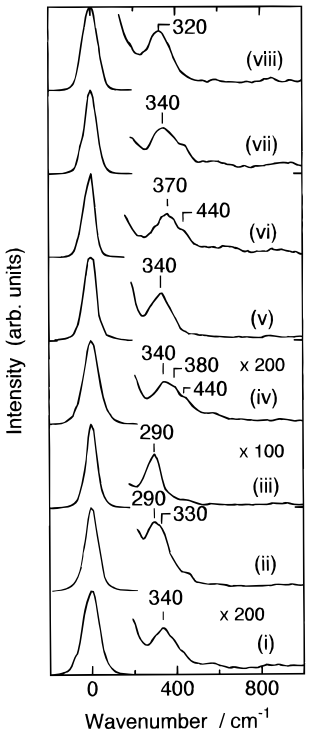


**Figure 1.** HREEL spectra measured at 100 K for Cu(100) surfaces covered with oxygen. Spectrum i was measured after Cu(100) was exposed to 50 langmuirs of oxygen at 300 K ($\theta_O$ = 0.11 ML). Spectra ii and iii were measured after exposing to 70 langmuirs (ii) and 300 langmuirs (iii) of oxygen at 500 K, resulting in oxygen coverages of 0.26 ML (ii) and 0.40 ML (iii). Spectrum iv was measured after exposing to 50 L of oxygen at 100 K ($\theta_O$ = 0.13 ML). Spectrum v was measured after the surface iv was annealed to 300 K. Spectrum (vi) was measured after exposing to 100 langmuirs of oxygen at 100 K ($\theta_O$ = 0.24 ML). Spectra vii and viii were measured after the surface vi was annealed to 200 K (vii) and 300 K (viii).

appeared at 290 cm$^{-1}$ in addition to the peak due to O(a) in the pseudo c(2×2)-O phase. The 290 cm$^{-1}$ peak is assigned to $\nu$(Cu−O) of O(a) in the $(\sqrt{2}\times2\sqrt{2})R45°$-O phase.[18] After further increasing coverage to 0.40 ML (iii), the 290 cm$^{-1}$ peak became sharp and the 330 cm$^{-1}$ peak was not definitely observed, indicating that the $(\sqrt{2}\times2\sqrt{2})R45°$-O phase was predominant at this oxygen coverage.

In a HREEL spectrum for an oxygen−as-exposed surface prepared by exposing to 50 L of oxygen at 100 K ($\theta_O$ = 0.13 ML), a peak was observed at 340 cm$^{-1}$ with a shoulder at 380 cm$^{-1}$ (iv). Considering the results in spectra i and ii, the 340 cm$^{-1}$ peak in iv is assigned to $\nu$(Cu−O) of O(a) in 4-fold hollow sites. The 380 cm$^{-1}$ peak is assigned to $\nu$(Cu−O) of O(a) in lower coordination sites such as bridge sites and atop sites in consideration of the higher frequency. A shoulder at 440 cm$^{-1}$ is assigned to $\nu$(Cu−OH) of OH(a) produced by dissociative adsorption of water in the residual gas, as described later in section 3.3. After annealing to 300 K (v), the 340 cm$^{-1}$ peak remained and the shoulder at 380 cm$^{-1}$ disappeared, indicating that oxygen atoms were accommodated in stable 4-fold hollow sites to produce the pseudo c(2×2) phase. At 100 langmuir exposure at 100 K ($\theta_O$ = 0.24 ML), the center of the $\nu$(Cu−O) peak shifted upward to 370 cm$^{-1}$, suggesting an increase of oxygen atoms on lower coordination sites (vi). A shoulder at 440 cm$^{-1}$ is assigned to $\nu$(Cu−OH) as mentioned above. After annealing the oxygen−as-exposed surface to 200 K (vii), the peak of $\nu$(Cu−O) moved downward to 340 cm$^{-1}$. Further annealing to 300 K caused a downward shift of $\nu$(Cu−O) to 320 cm$^{-1}$ (viii). The downward shift of $\nu$(Cu−O) in the spectra vi−viii on annealing to 300 K is attributed to the growth of the

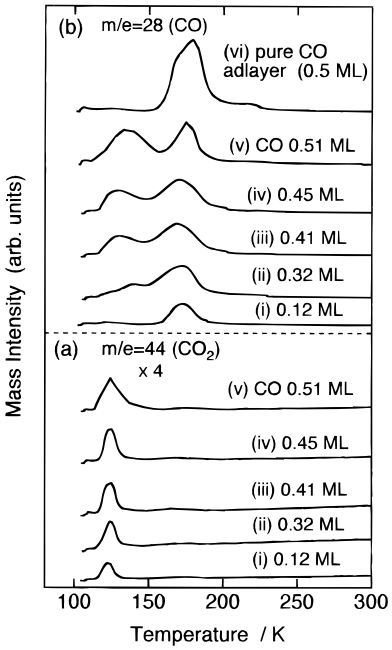


**Figure 2.** TPD spectra for $m/e = 44$ ($CO_2$) (a) and $m/e = 28$ (CO) (b) from Cu(100). Spectra i−v were measured after Cu(100) was exposed to 50 langmuirs of oxygen at 100 K ($\theta_O = 0.13$ ML) and subsequently exposed to various amounts of CO at 100 K. CO coverages were 0.12 ML (i), 0.32 ML (ii), 0.41 ML (iii), 0.45 ML (iv), and 0.51 ML (v). Spectrum vi in part b was measured after exposing Cu(100) to 1.8 L of CO at 100 K.

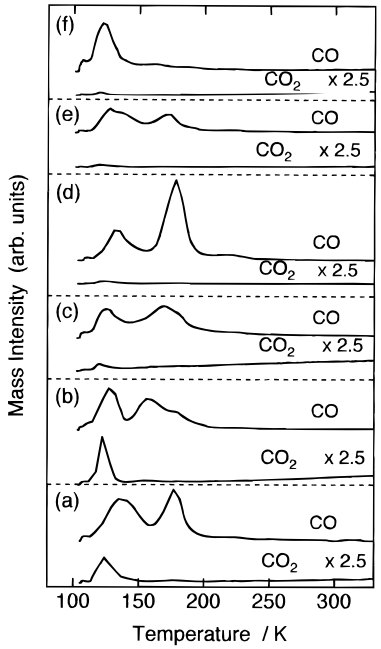


**Figure 3.** TPD spectra for $m/e = 44$ ($CO_2$) and $m/e = 28$ (CO) from O−CO coadlayers on Cu(100). Parts a and b were obtained after the oxygen−as-exposed surfaces ($\theta_O = 0.13$ ML (a) and 0.24 ML (b)) were exposed to 6.0 langmuirs of CO at 100 K. Part c was obtained after the as-exposed surface ($\theta_O = 0.24$ ML) was preannealed to 300 K (c) and cooled down to 100 K followed by exposing to 6.0 langmuirs of CO. Parts d−f were obtained after the pseudo c(2×2)-O phase ($\theta_O = 0.15$ ML), a mixture of the pseudo c(2×2)-O and the $(\sqrt{2}\times2\sqrt{2})R45°$-O phases ($\theta_O = 0.26$ ML), and the $(\sqrt{2}\times2\sqrt{2})R45°$-O phase ($\theta_O = 0.45$ ML) were exposed to 6.0 langmuirs of CO at 100 K.

both pseudo c(2×2)-O and $(\sqrt{2}\times2\sqrt{2})R45°$-O phases according to the explanation of Wuttig et al.[18]

In the present study, oxygen adlayers were prepared on the basis of the results of Figure 1 as follows. The as-exposed surface was prepared by exposing to 50−100 langmuirs of oxygen at 100 K. The pseudo c(2×2)-O phase and the $(\sqrt{2}\times2\sqrt{2})R45°$-O phase were obtained by exposing to 50−100 langmuirs of oxygen at 300 K and to 300 −500 langmuirs of oxygen at 500 K, respectively. The oxygen coverage corresponded to 0.11−0.15 ML and 0.40−0.45 ML. A mixture of the pseudo c(2×2)-O and the $(\sqrt{2}\times2\sqrt{2})R45°$-O phases ($\theta_O = 0.26$ ML) was prepared by exposing to 70 langmuirs of oxygen at 500 K.

**3.2. O−CO Coadlayers.** In order to investigate the reactivity of oxygen atoms in the oxygen−as-exposed surfaces for CO oxidation, TPD experiments were performed. Figure 2 shows TPD spectra measured after exposing the oxygen−as-exposed surface ($\theta_O = 0.13$ ML) to various amounts of CO at 100 K. As shown in Figure 2a, $CO_2$ desorbed at 125 K in a wide range of CO coverage from 0.12 to 0.51 ML. The amount of desorbed $CO_2$ increased with increasing CO coverage and reached 0.039 ML at 0.51 ML of CO(a) (Figure 2a (v)). TPD spectra of CO are shown in Figure 2b. From an O−CO coadlayer with 0.12 ML of CO(a) (Figure 2b (i)), the CO desorption peak was observed at 175 K. This desorption feature is similar to that from a pure CO adlayer as shown in vi. At 0.32 ML of CO(a) (ii), a new peak appeared at 140 K. With further increasing CO coverage (iii−v), the component of CO desorption below 150 K increased.

The change in the reactivity of oxygen atoms on annealing the as-exposed surface to 300 K was investigated as shown in Figure 3 a−c. TPD spectra in Figure 3a,b were obtained after the as-exposed surfaces with 0.13 ML (a) and 0.24 ML (b) of oxygen were exposed to CO at 100 K. The results for the as-exposed surfaces that were preannealed before CO exposure at 100 K are shown in Figures 3c. In the case of the oxygen−as-exposed surface without preannealing (a and b), a $CO_2$ desorption peak was observed at 125 K. The desorbed $CO_2$ amounted to 0.039 ML (a) and 0.051 ML (b). By preannealing the as-exposed surface with 0.24 ML of oxygen to 300 K (c), the amount of desorbed $CO_2$ decreased to 0.005 ML (c). In contrast to the large decrease of $CO_2$ production by the preannealing, the change in the amount of adsorbed CO was relatively small; the CO coverages were 0.46 ML (a), 0.41 ML (b), and 0.37 ML (c). The results in Figure 3a−c indicate that the high reactivity of oxygen atoms in the as-exposed surfaces for CO oxidation decreased by preannealing to 300 K.

The reactivities of oxygen atoms in the pseudo c(2×2) phase, the $(\sqrt{2}\times2\sqrt{2})R45°$-O phase, and the mixture of these phases are shown in Figure 3d−f. The amounts of $CO_2$ production were very small; 0.002 ML from the pseudo c(2×2) phase (d), 0.003 ML from the mixture (e), and 0.001 ML from the $(\sqrt{2}\times2\sqrt{2})R45°$-O phase (f). It should be noted that CO oxidation by oxygen atoms formed above 300 K was reported only at surface temperatures of 473−623 K under exposure to $2.6 \times 10^{-4}$ to $1.3 \times 10^{-2}$ Pa of CO[27,28] and of 300 K under exposure to $1.2 \times 10^{3}$ Pa of CO.[29] The amounts of adsorbed CO were 0.46 ML (d), 0.21 ML (e), and 0.05 ML (f). The decrease in the amount of CO adsorption is ascribed to site blocking by oxygen.

**3.3. Dissociative Adsorption of Water on Oxygen-Precovered Cu(100).** The adsorption and reaction of water on the as-exposed surface, the pseudo c(2×2)-O phase, the $(\sqrt{2}\times2\sqrt{2})R45°$-O phase, and the mixture of the pseudo c(2×2) and the $(\sqrt{2}\times2\sqrt{2})R45°$-O phases were investigated by TPD and HREELS.

*3.3.1. TPD.* Figure 4a shows TPD spectra for $H_2O$ desorption from pure water adlayers on Cu(100). At 0.05 langmuir (Figure 4a (i)), the desorption peak appeared at 170 K ($\alpha_1$). A

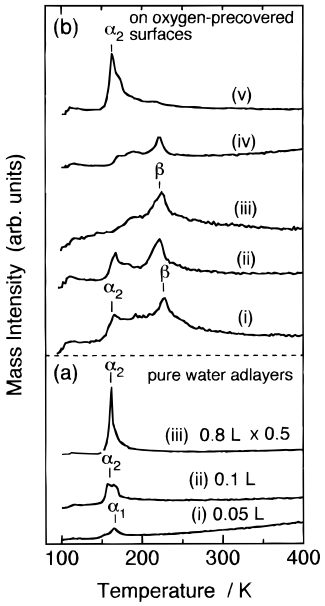


**Figure 4.** (a) TPD spectra for $m/e = 18$ ($H_2O$) from the pure water layer on Cu(100). Spectra i−iii were measured after Cu(100) was exposed to 0.05 langmuir (i), 0.1 langmuir (ii), and 0.8 langmuir (iii) of water at 100 K. (b) TPD spectra for $m/e = 18$ ($H_2O$) measured after oxygen-precovered Cu(100) was exposed to water at 100 K. Spectra i and ii were measured after the as-exposed surfaces ($\theta_O = 0.13$ ML (a) and 0.24 ML (b)) were exposed to 0.5 langmuir of water at 100 K. Spectra iii−v were measured after the pseudo c(2×2)-O phase, the mixture of the pseudo c(2×2)-O and the $(\sqrt{2}\times2\sqrt{2})R45°$-O phases ($\theta_O = 0.26$ ML), and the $(\sqrt{2}\times2\sqrt{2})R45°$-O phase ($\theta_O = 0.45$ ML) were exposed to 0.5 langmuir of water at 100 K.

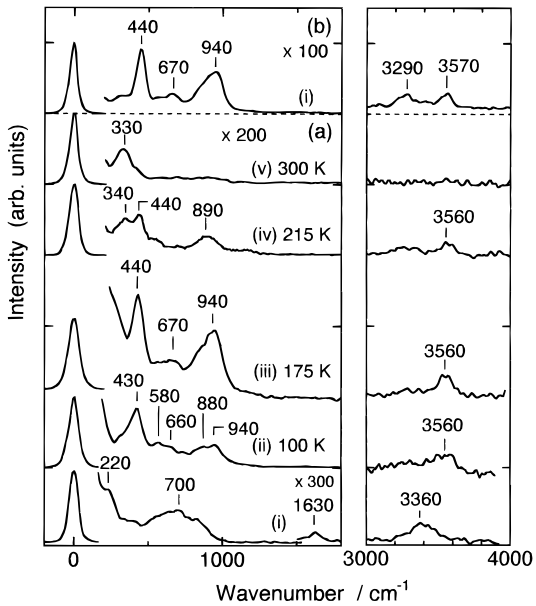


**Figure 5.** HREEL spectra measured after the oxygen−as-exposed surfaces ($\theta_O = 0.13$ ML (a) and 0.24 ML (b)) were exposed to water at 100 K and annealed to given temperatures, followed by cooling to 100 K. A spectrum for a pure water adlayer is also shown in part a for comparison. (a) Spectrum i was measured after exposing Cu(100) to 0.5 langmuir of water at 100 K. Spectrum ii was measured after the as-exposed surface ($\theta_O = 0.13$ ML) was exposed to 0.2 langmuir of water at 100 K. Spectra iii−v were measured after the surface ii was annealed to 175 K (iii), 215 K (iv), and 300 K (v). (b) Spectrum i was measured after the as-exposed surface ($\theta_O = 0.24$ ML) was exposed to 0.5 langmuir of water at 100 K followed by annealing to 175 K.

new peak grew at 160 K ($\alpha_2$) at 0.1 langmuir (ii) and gained in intensity with increasing exposure to 0.8 langmuir (iii). Brosseau et al. attributed the $\alpha_2$ peak as desorption from the water multilayer and the $\alpha_1$ peak as desorption induced by defect sites.[35] Another possible interpretation is that the $\alpha_2$ peak and the $\alpha_1$ peak correspond to the multilayer and the first (chemisorbed) layer, respectively, as reported for Pd(100),[36] Ru(001),[37] and Cu(110).[38] It is to be noted that desorption of the multilayer water in TPD was observed at 150−160 K from various metal surfaces.[8]

Figure 4b shows TPD spectra measured after Cu(100) surfaces with precovered oxygen were exposed to 0.5 langmuir of $H_2O$ at 100 K. In spectra i and ii obtained for the as-exposed surfaces with 0.13 ML (i) and 0.24 ML (ii) of precovered oxygen, a new peak appeared at 225 K ($\beta$) in addition to the $\alpha_2$ peak. The $\beta$ peak is attributed to a recombinative desorption peak due to disproportionation of OH(a) produced by dissociative adsorption of water, as described later in section 3.3.2. A small rise at 110 K is ascribed to sublimation of water from the sample holder, which was verified with changing the relative position of the sample to QMS in the TPD measurement. The $\beta$ peak was also observed in the result for the pseudo c(2×2)-O phase (iii). In spectrum iv for a mixture of the pseudo c(2×2) and $(\sqrt{2}\times2\sqrt{2})R45°$-O phases, the area of the $\beta$ peak decreased as compared with those in spectra ii and iii. In spectrum v measured for the $(\sqrt{2}\times2\sqrt{2})R45°$-O phase, the $\beta$ peak was hardly distinguishable, while the $\alpha_2$ peak due to desorption of the multilayer was observed at 160 K. The results in Figure 4b mean that disproportionation of OH(a) and/or dissociative adsorption of water were suppressed on the $(\sqrt{2}\times2\sqrt{2})R45°$-O phase, which is verified by means of HREELS in the next section.

*3.3.2. HREELS.* Figure 5a,b shows HREEL spectra measured after the oxygen−as-exposed surfaces were exposed to water at 100 K and subsequently annealed to given temperatures. The oxygen precoverages were 0.13 ML in Figure 5a and 0.24 ML in Figure 5b. A HREEL spectrum for the pure water adlayer is shown in Figure 5a (i) for comparison. In spectrum i, four peaks were observed at 220, 700, 1630, and 3360 $cm^{-1}$. Vibrational features of water on metal surfaces are summarized in Table 1. In consideration of the previous studies, the four peaks are assigned to frustrated translation, frustrated rotation, the scissoring mode ($\delta$(HOH)), and $\nu$(O−H), respectively.

After the oxygen−as-exposed surface was exposed to 0.2 langmuir of water (ii), the $\nu$(Cu−O) mode was not distinguishable. Instead, five peaks appeared at 430, 580, 880, 940, and 3560 $cm^{-1}$ with a shoulder at 660 $cm^{-1}$. Vibrational spectra for OH(a) on other metal surfaces are summarized in Table 2. According to these studies, the 430 $cm^{-1}$ peak and the 3560 $cm^{-1}$ peak are assigned to $\nu$(Cu−OH) and $\nu$(O−H), respectively, and the peaks at 880 and 950 $cm^{-1}$ are assigned to $\delta$(O−H). The 580 $cm^{-1}$ peak is assigned to frustrated lateral translation of OH(a) as reported on Rh(100)[48] and Pd(100).[36] The weak peak at 660 $cm^{-1}$ is ascribed to frustrated rotation of water in consideration of Table 1. The result of Figure 5a (ii) indicates that dissociative adsorption of water via hydrogen abstraction by O(a) occurred even at 100 K according to the following step:

$$O(a) + H_2O(a) \rightarrow 2OH(a) \qquad (1)$$

After annealing to 175 K (iii), four peaks were observed at 440 $cm^{-1}$ ($\nu$(Cu−OH) of OH(a)), 670 $cm^{-1}$ (frustrated rotation of water), 940 $cm^{-1}$ ($\delta$(O−H) of OH(a)), and 3560 $cm^{-1}$ ($\nu$(O−H) of OH(a)). After further annealing to 215 K (iv), the peak intensity of $\nu$(Cu−OH) decreased and the $\nu$(Cu−O) mode of O(a) appeared again at 340 $cm^{-1}$. The peak of $\delta$(O−H) also decreased in intensity, and the peak position moved downward

**TABLE 1: Vibrational Frequencies (in $cm^{-1}$) of $H_2O$ Adsorbed on Various Metal Surfaces**

| surface | $\nu$(M−$OH_2$) | frustrated translation | frustrated rotation | $\delta$(HOH) | $\nu$(O−H···M) | $\nu$(O−H···O) | $\nu$(OH) | ref |
|---|---|---|---|---|---|---|---|---|
| Pt(111) | 550 | 250 | 700 | 1625 | n.o. | 3400 | n.o. | 39 |
| | n.o. | 260 | 660, 945 | 1620 | n.o. | 3400 | n.o. | 40 |
| Pd(100) | 335 | n.o. | n.o. | 1560 | n.o. | n.o. | n.o. | 41[a] |
| | n.o. | n.o. | 815−835 | 1640 | n.o. | 3375−3460 | n.o. | 36 |
| | n.o. | 220 | 610, 810 | 1600 | n.o. | 3400 | n.o. | 42 |
| Ru(001) | n.o. | 230 | 750[b] | 1650 | n.o. | 3420 | n.o. | 37 |
| | 390 | n.o. | 680−700, 890−930[c] | 1520 | 2935 | 3400 | 3565 | 37 |
| Ni(100) | n.o. | 230 | 530, 760 | 1610 | 3030 | 3350 | 3660 | 43 |
| Fe(100) | n.o. | n.o. | 690[b] | 1630 | 3070 | 3380 | n.o. | 44 |
| Al(111) | 660 | 215−240 | 785 | 1655 | n.o. | 3445 | n.o. | 45 |
| Ag(110) | n.o. | 200 | 740[b] | 1660 | n.o. | 3410 | n.o. | 46 |
| Cu(100) | 230 | n.o. | n.o. | 1590 | n.o. | n.o. | n.o. | 41[a] |
| | n.o. | 220 | 600, 800 | 1600 | n.o. | n.o. | n.o. | 14 |
| | n.o. | 230−250 | 610−780[b,d] | 1610 | n.o. | 3370−3410 | n.o. | 35 |
| | n.o. | 220 | 700[b] | 1630 | n.o. | 3360 | n.o. | this study |

[a] Water monomers prepared at 10 K without intermolecular hydrogen bonding. [b] Broad feature. [c] The former corresponds to the multilayer and the latter corresponds to the bilayer. [d] The peak position depends on exposure. This peak is suggested to be a superposition of the peaks at 610 and 810 $cm^{-1}$. [e] n.o.: not observed.

**TABLE 2: Vibrational Frequencies (in $cm^{-1}$) of OH(a) on Various Metal Surfaces**

| surface | $\nu$(M−OH) | frustrated translation | $\delta$(O−H) | $\nu$(O−H) | ref |
|---|---|---|---|---|---|
| Pt(111) | 430 | n.o.[a] | 1015 | 3480 | 47 |
| Pd(100) | 445 | 660 | 930 | 3250 | 36 |
| | 440 | n.o. | 930 | 3160 | 42 |
| Rh(100) | 440 | 660 | 920 | 3180 | 48 |
| Ni(110) | 350 | 620 | 950 | 3580 | 43 |
| Fe(100) | 470 | n.o. | 1190 | 3620 | 44 |
| Al(111) | 765−780 | n.o. | n.o. | 3710−3745 | 45 |
| Ag(110) | 280 | n.o. | 930 | 3250 | 46 |
| Ag(100) | 300 | n.o. | 670 | 3380 | 14 |
| Cu(100) | 420 | n.o. | 850−900 | 3620 | 14[b] |
| | 430−440 | 580 | 880−940 | 3560 | this work |

[a] n.o.: not observed. [b] A water-precovered Cu(100) surface was annealed to 180−220 K under oxygen of $1.3 \times 10^{-5}$ Pa.

to 890 $cm^{-1}$. After annealing to 300 K (v), the peaks associated with OH(a) diminished and the $\nu$(Cu−O) mode grew at 330 $cm^{-1}$. Since this behavior corresponds to the $\beta$ desorption peak of water at 225 K in Figure 4b, it is deduced that the $\beta$ peak results from disproportionation of OH(a):

$$2OH(a) \rightarrow H_2O + O(a) \qquad (2)$$

The result for the as-exposed surface with 0.24 ML of oxygen is shown in Figure 5b, where the formation of OH(a) was also detected. After exposing to 0.5 langmuir of water and annealing to 175 K, peaks associated with OH(a) appeared at 440 $cm^{-1}$ ($\nu$(Cu−OH)), 940 $cm^{-1}$ ($\delta$(O−H)), and 3570 $cm^{-1}$ ($\nu$(O−H)). Peaks at 670 and 3290 $cm^{-1}$ are assigned to frustrated rotation and $\nu$(O−H) of the remaining water molecules, respectively.

Figure 6a shows HREEL spectra measured after the pseudo c(2×2)-O phase was exposed to water at 100 K and annealed to each temperature. The results are similar to those in Figure 5a,b. After exposing the pseudo c(2×2)-O phase to 0.5 langmuir water at 100 K (Figure 6a (i)), the intensity of the $\nu$(Cu−O) mode became faint and the peaks associated with OH(a) were observed at 440 $cm^{-1}$ ($\nu$(Cu−OH)), 930 $cm^{-1}$ ($\delta$(OH)), and 3560 $cm^{-1}$ ($\nu$(O−H)). A broad peak centered at 3270 $cm^{-1}$ is assigned to $\nu$(O−H) of water. This result indicates that adsorbed oxygen in the pseudo c(2×2)-O phase abstracted hydrogen of water at 100 K to produce OH(a) according to step 1. After annealing to 175 K (ii), the $\delta$(OH) mode was observed at 940 $cm^{-1}$, and its normalized intensity increased. The $\nu$(Cu−OH) mode and $\nu$(O−H) mode appeared at 440 and 3560 $cm^{-1}$. At 225 K (iii), the intensities of the peaks associated with OH(a)

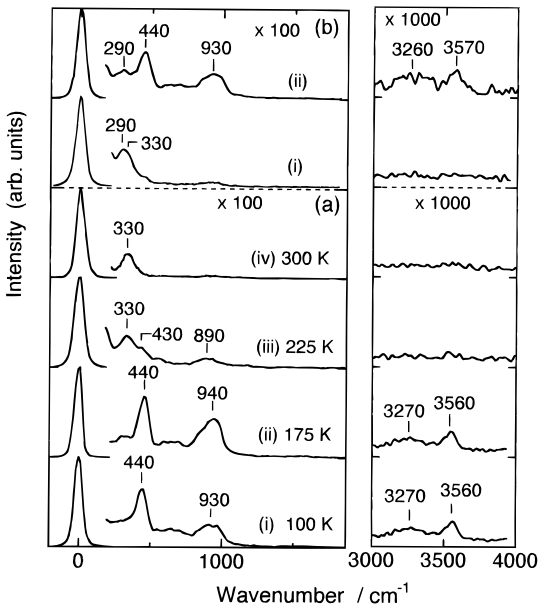


**Figure 6.** HREEL spectra measured after Cu(100) with precovered oxygen was exposed to water at 100 K and annealed to given temperatures followed by cooling down to 100 K. (a) Spectrum i was measured after the pseudo c(2×2)-O phase ($\theta_O$ = 0.15 ML) was exposed to 0.5 langmuir of water at 100 K. Spectra ii−iv were measured after the surface i was annealed to 175 K (ii), 225 K (iii), and 300 K (iv). (b) Spectrum i was measured for the mixture of the pseudo c(2×2)-O and the ($\sqrt{2}\times2\sqrt{2}$)*R*45°-O phases ($\theta_O$ = 0.26 ML). Spectrum ii was measured after the surface i was exposed to 0.2 langmuir of oxygen at 100 K and annealed to 175 K.

decreased and the $\nu$(Cu−O) mode appeared at 330 $cm^{-1}$ after disproportionation of OH(a) and desorption of OH(a) (step 2). The peak position of $\delta$(OH) shifted downward to 890 $cm^{-1}$ at 225 K. Further annealing to 300 K caused complete disappearance of the peaks associated with OH(a) (iv).

Figure 6b shows the results for the mixture of the pseudo c(2×2) phase and the ($\sqrt{2}\times2\sqrt{2}$)*R*45°-O phase. After exposing to water at 100 K and annealing to 175 K, new peaks associated with OH(a) were observed at 440, 930, and 3570 $cm^{-1}$.

The results for the ($\sqrt{2}\times2\sqrt{2}$)*R*45°-O phase are shown in Figure 7. After exposing to water at 100 K i and ii, frustrated rotation and $\nu$(O−H) peaks for water were observed at 690−710 $cm^{-1}$ and 3350 $cm^{-1}$, respectively. Subsequent annealing to 175 K (iii) caused disappearance of the peaks associated with water. Instead, peaks associated with OH(a) appeared at 440 $cm^{-1}$ ($\nu$(Cu−OH)) and 930 $cm^{-1}$ ($\delta$(OH)) with much smaller

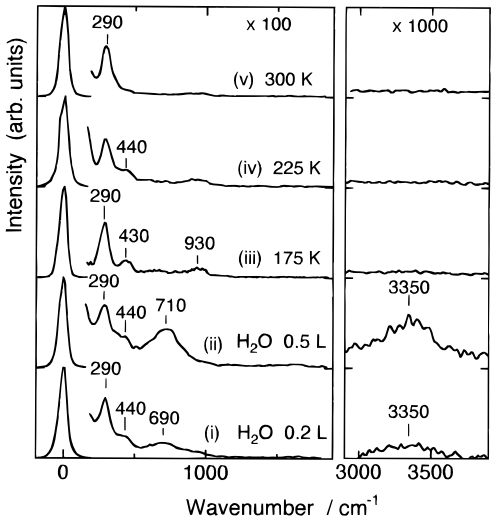


**Figure 7.** HREEL spectra measured after the $(\sqrt{2}\times2\sqrt{2})R45°$-O phase was exposed to water at 100 K and annealed to given temperatures followed by cooling to 100 K. Spectra i and ii were measured after the $(\sqrt{2}\times2\sqrt{2})R45°$-O phase was exposed to 0.2 langmuir (i) and 0.5 langmuir (ii) of water at 100 K. Spectra iii−v were measured after the surface (ii) was annealed to 175 K (iii), 225 K (iv), and 300 K (v).

intensities than those on the as-exposed surface (Figure 5) and the pseudo c(2×2) phase (Figure 6). The small intensities of the peaks for OH(a) in Figure 7 (iii) are in agreement with the TPD result in Figure 4b (v), where the recombinative desorption peak (the $\beta$ peak) was hardly distinguishable. Accordingly, it is concluded that the OH(a) formation was suppressed largely on the $(\sqrt{2}\times2\sqrt{2})R45°$-O phase. The peaks associated with OH(a) disappeared on annealing to 300 K (iv and v). The 290 $cm^{-1}$ peak characteristic of the $(\sqrt{2}\times2\sqrt{2})R45°$-O phase remained with a large intensity in all conditions (i−v).

## 4. Discussion

**4.1. CO Oxidation on Cu(100).** As shown in Figure 2, $CO_2$ production was observed at 125 K in TPD spectra measured after the oxygen−as-exposed surfaces formed at 100 K were exposed to CO. After annealing the as-exposed surface to 300 K before CO adsorption, the $CO_2$ formation was drastically reduced to one-tenth. The decrease in the reactivity corresponds to the growth of the pseudo c(2×2)-O phase and the $(\sqrt{2}\times2\sqrt{2})R45°$-O phase, as indicated in the vibrational spectra (vi−viii) in Figure 1. The lower reactivity of the oxygen atoms in the pseudo c(2×2)-O phase and the $(\sqrt{2}\times2\sqrt{2})R45°$-O phase is also evident in Figure 3d−f. These results suggest that the reactive species for CO oxidation on Cu(100) are metastable oxygen atoms in the as-exposed surfaces before becoming accommodated in thermally stable states. The metastable oxygen atoms in the disordered as-exposed surfaces seem to be in a higher energy state and require a smaller activation energy for CO oxidation than the oxygen atoms in the pseudo c(2×2)-O and $(\sqrt{2}\times2\sqrt{2})R45°$ phases. The possible sites where metastable oxygen atoms are located are the atop site, bridge site, and 4-fold hollow site. The assignment for the site of metastable oxygen responsible for the reactivity remains to be solved. It is noted that as-exposed oxygen on Cu(111) at 110 K cannot react with CO and that CO adsorption is not affected by coadsorbed oxygen, indicating that as-exposed oxygen on 3-fold hollow site is not reactive.[5]

The high reactivity of oxygen atoms prepared at low temperatures has also been reported on Ni(210), Cu(110), and Pt(111). Carley et al. reported that oxygen adatoms formed on Ni(210) at 77 K were in a transient state without strong bonds to metal atoms and were more reactive for H-abstraction than the oxygen atoms formed at 297 K.[49] We have reported that oxygen atoms formed on unreconstructed Cu(110) below 230 K have high reactivity for CO oxidation in TPD and for catalytic CO oxidation, and the reactivity decreased by annealing above 250 K, where the reconstructed (2×1)-O structure was produced.[4−7] The oxygen atoms on unreconstructed Cu(110) were also reactive for hydrogenation of $NH_3$(a) to produce $NH_2$(a), NH(a), and N(a), while the oxygen atoms in the reconstructed (2×1)-O structure were inert for the reaction.[50] More recently, the reactivity of oxygen atoms on Pt(111) in a disordered phase, which was prepared by exposing the Pt(111) surface to oxygen below 100 K and annealing to 150 K, was compared with the reactivity of oxygen atoms in the p(2×2)-O phase produced by further annealing to 350 K.[51,52] For the CO oxidation from O−CO coadlayers, the oxygen atoms in the disordered phase caused a $CO_2$ desorption peak at lower temperature than those in the p(2×2) phase.[51] The oxygen atoms in the disordered phase were also reactive for oxygen-exchange reaction between NO(a) and O(a), although those in the p(2×2) phase were not reactive.[52]

On Pt and Pd, which are regarded as the most reactive metals for oxidation, CO oxidation by oxygen atoms in ordered phases prepared by annealing oxygen adlayers above 300 K has been investigated.[53−59] In these studies, $CO_2$ desorption peaks were observed between 300 and 500 K at low total coverage of O(a) and CO(a). With increasing total coverage, new peaks appeared at lower temperatures because of repulsive interactions between the adsorbates. Desorption peaks appeared below 300 K only when the total coverage of O(a) and CO(a) exceeded a threshold coverage: 0.56 ML for Pt(110)-(1 × 2),[54,55] 0.5 ML for Pd(100),[56,57] and 1 ML for Pd(111).[58] In contrast, $CO_2$ production from the as-exposed Cu(100) surfaces was observed at 125 K even at a total coverage as small as 0.25 ML, as shown in Figure 2a (i). $CO_2$ production below 200 K was also observed for the as-exposed Cu(110) surface at a total coverage of 0.13 ML.[4,5] On the basis of these studies, the reactivity of metastable oxygen atoms on Cu is suggested to be higher than the reactivity of oxygen atoms prepared above room temperature on Pt and Pd.

**4.2. The Bonding Structure of OH(a) on Cu(100).** The intense peak of $\delta$(O−H) in Figures 5 and 6 indicates that the O−H axis of OH(a) was inclined with respect to the surface normal on Cu(100). With regard to the bonding geometry of OH(a), the bent configuration of OH(a) on atop sites was ascribed to hybridization between metal d states and OH 1$\pi$ orbitals derived from O 2p states, whereas OH(a) on multiple coordination sites was suggested to be in a linear configuration.[8,60] Recently Canepa et al. investigated Ag(110) covered with bent OH(a) by means of ARUPS and assigned the dispersion of 2−4 eV to antibonding levels caused by hybridization between OH 1$\pi$ orbitals and Ag 4d states.[61] Therefore, the bent configuration of OH(a) on Cu(100) seems to be favored by the $\pi$−d hybridization. The effect of hydrogen bonding between OH(a) on the configuration is probably small on Cu(100) since hydrogen bonding would cause lower frequencies of $\nu$(O−H) than the frequency observed in Figures 5 and 6.[8,36]

The feature of the $\delta$(O−H) mode was affected by annealing from 100 to 225 K, as shown in Figure 5a. On annealing from 100 to 175 K (spectra ii and iii in Figure 5a), the peak intensity normalized to the elastic peak increased remarkably from 0.09% to 0.35%, although a smaller increase from 0.25% to 0.35% was observed for the peak assigned to $\nu$(Cu−OH). Similar results were also observed in Figure 6. Since the bent configuration was preferred on atop sites as mentioned above,

the increase of the peak intensity of $\delta$(O−H) on annealing is attributed to enhanced occupation of atop sites. Further annealing to 215 K caused the downward shift of the peak position from 940 to 890 $cm^{-1}$ (Figure 5a (iv)), suggesting a change in the hybridization between OH 1$\pi$ orbitals and Cu 3d states. The change in the $\pi$−d hybridization is ascribed to accumulation of adsorbed oxygen due to disproportionation of OH(a) (step 2); accumulated O(a) acts as an electronegative additive and charge transfer from Cu 3d states to O(a) occurs, leading to weakening of the $\pi$−d hybridization. The broadening on the low-frequency side of the 940 $cm^{-1}$ peak at 100−175 K (spectra ii and iii in Figure 5a) is possibly due to a small amount of remaining O(a).

**4.3. Hydrogen Abstraction from Water by Precovered Oxygen on Cu(100).** As shown in Figures 5 and 6, hydrogen abstraction from postdosed water occurred even at 100 K on the as-exposed surface (Figure 5) and the pseudo c(2×2)-O surface (Figure 6). The $\nu$(Cu−O) mode became faint in OH(a) formation via hydrogen abstraction in Figures 5 and 6, suggesting that most of adsorbed oxygen in the as-exposed surfaces and the pseudo c(2×2)-O phase abstracted hydrogen from water and changed to OH(a). The $\nu$(Cu−O) mode reappeared with a large intensity by recombinative desorption of OH(a). The pseudo c(2×2) phase is active for the hydrogen abstraction, whereas this phase is inert in CO oxidation as mentioned in section 4.1. On the ($\sqrt{2}\times2\sqrt{2}$)*R*45°-O phase comprised of −Cu−O− chains along the [001] direction, hydrogen abstraction was suppressed remarkably (Figure 7), suggesting that the reactivity of oxygen atoms for hydrogen abstraction decreased by incorporation into the −Cu−O− chains.

For the hydrogen abstraction from $NH_3$,[12,62] water,[38,63] and methanol[64] on Cu(110), from $NH_3$ on Ni(110),[65−68] and from $H_2O$ on Cu(111),[69] it has been reported that adsorbed oxygen acts as a promoter at low coverages, although adsorbed oxygen becomes inert at high coverages. This dependence of the reactivity on oxygen coverage was investigated in detail for water on Cu(110) by Bange et al.[38] They reported that the amount of OH(a) increased linearly with increasing oxygen coverage up to 0.13 ML, decreased largely above 0.13 ML, and became almost zero at 0.25−0.30 ML. Recently the change in reactivity of oxygen atoms has been found to be related to the surface reconstruction induced by oxygen adsorption in STM studies for $NH_3$ on Ni(110)[9] and for methanol on Cu(110).[10,11] In the STM studies,[9−11] oxygen atoms at the ends of the −metal−O− chains in the reconstructed phases were suggested to be active for hydrogen abstraction, while oxygen atoms in the chains with two metal neighbors were inert. A similar conclusion was obtained for $NH_3$ on Cu(110) by comparison with experimental results and Monte Carlo simulation.[12,50,62,67,69] In their simulation, reactive oxygen atoms, which were isolated or at the perimeter of the island, were produced at low coverage, and oxygen atoms in the islands were not reactive.

The results on Cu(100) in the present study can also be explained in relation to the adsorbate-induced reconstruction; oxygen atoms in the ($\sqrt{2}\times2\sqrt{2}$)*R*45°-O phase were incorporated into the chains with strong Cu−O bonds parallel to the surface and not reactive for the hydrogen abstraction. It should be noted that the Cu(100)-($\sqrt{2}\times2\sqrt{2}$)*R*45°-O phase consists of −metal−O− chains along the [001] direction similarly to Cu(110)-(2×1)-O and Ni(110)-O phases.[70−73] The small amount of OH(a) detected in Figure 7 would be ascribed to oxygen atoms at the ends of the −Cu−O− chains.

The OH(a) formation on Cu(100) was examined by Spitzer et al.[13] and Carley et al.[14] Spitzer et al. reported by means of UPS that OH formation occurred after the Cu(100) surface with precovered oxygen formed at 300 K was exposed to water at 100 K followed by annealing above 150 K, although the spectra were not shown.[13] On the basis of the results in the present study, it is deduced that oxygen atoms in the pseudo c(2×2)-O phase and/or at the perimeter of the ($\sqrt{2}\times2\sqrt{2}$)*R*45°-O phase contributed to OH(a) formation in their conditions. Carley et al. measured HREEL spectra after Cu(100) with the multilayer of water was annealed to 180−220 K in exposure to $1.5 \times 10^{-3}$ Pa of oxygen and assumed that the reactive species for OH(a) formation was transient molecular oxygen.[14] However, they did not exclude the possibility that coadsorbed water enhanced dissociation of the O−O bond of molecular oxygen and that oxygen atoms were the reactive species. Our results suggest that atomic oxygen is responsible for the hydrogen abstraction.

## 5. Summary

The reactivity of oxygen atoms in the as-exposed surfaces formed at 100 K for CO oxidation was found to be higher than that of oxygen atoms in the pseudo c(2×2)-O phase and the ($\sqrt{2}\times2\sqrt{2}$)*R*45°-O phase. The reactivity of metastable oxygen atoms on Cu(110) and Cu(100) may be higher than that of oxygen atoms adsorbed on Pt and Pd. The change from the as-exposed surface to the pseudo c(2×2)-O and ($\sqrt{2}\times2\sqrt{2}$)-*R*45°-O phases by annealing was indicated in the feature of $\nu$(Cu−O) in HREEL spectra. With regard to hydrogen abstraction from water, isolated oxygen atoms in the as-exposed surface and the pseudo c(2×2)-O phase were reactive and produced OH(a) after exposure to water even at 100 K. On annealing the surface covered with OH(a), the recombinative desorption of OH(a) was observed at 225 K. In contrast, the OH(a) formation was remarkably suppressed when the oxygen atoms were incorporated into −Cu−O− chains along the [001] direction in the ($\sqrt{2}\times2\sqrt{2}$)*R*45°-O phase.

**Acknowledgment.** This work has been supported by CREST (Core Research for Evolutional Science and Technology) of Japan Science and Technology Corporation (JST).

## References and Notes

(1) Engel, T.; Ertl, G. *Adv. Catal.* **1979**, *28*, 1.
(2) Prasad, R.; Kennedy, L.; Ruckenstein, E. *Catal. Rev. Sci. Eng.* **1984**, *26*, 1.
(3) Jernigan, G. G.; Somorjai, J. *J. Catal.* **1994**, *147*, 567.
(4) Sasaki, T.; Sueyoshi, T.; Iwasawa, Y. *Surf. Sci.* **1994**, *316*, L1081.
(5) Sueyoshi, T.; Sasaki, T.; Iwasawa, Y. *Surf. Sci.* **1995**, *343*, 1.
(6) Sueyoshi, T.; Sasaki, T.; Iwasawa, Y. *Chem. Phys. Lett.* **1995**, *241*, 189.
(7) Sueyoshi, T.; Sasaki, T.; Iwasawa, Y. *J. Phys. Chem.* **1996**, *100*, 1048.
(8) Thiel, P. A.; Madey, T. E. *Surf. Sci. Rep.* **1987**, *7*, 211.
(9) Ruan, L.; Stensgaard, I.; Lægsgaard, E.; Besenbacher, F. *Surf. Sci.* **1994**, *314*, L873.
(10) Francis, S. M.; Leibsle, F. M.; Haq, S.; Xiang, N.; Bowker, M. *Surf. Sci.* **1994**, *315*, 284.
(11) Leibsle, F. M.; Francis, S. M.; Davis, R.; Xiang, N.; Haq, S.; Bowker, M. *Phys. Rev. Lett.* **1994**, *72*, 2569.
(12) Carley, A. F.; Davies, P. R.; Roberts, M. W.; Vincent, D. *Top. Catal.* **1994**, *1*, 35.
(13) Spitzer, A.; Ritz, A.; Lüth, H. *Surf. Sci.* **1985**, *152/153*, 543.
(14) Carley, A. F.; Davies, P. R.; Roberts, M. W.; Thomas, K. K. *Surf. Sci. Lett.* **1990**, *238*, L467.
(15) Mayer, R.; Zhang, C.-S.; Lynn, K. G. *Phys. Rev. B* **1986**, *33*, 8899.
(16) Wöll, C.; Wilson, R. J.; Chiang, S.; Zeng, H. C.; Mitchell, K. A. R. *Phys. Rev. B* **1990**, *42*, 11926.
(17) Mohamed, M. H.; Kesmodel, L. L. *Surf. Sci. Lett.* **1987**, *185*, L467.
(18) Wuttig, M.; Franchy, G.; Ibach, H. *Surf. Sci.* **1989**, *213*, 103.
(19) Asensio, M. C.; Ashwin, M. J.; Kilcoyne, A. L. D.; Woodruff, D. P.; Robinson, A. W.; Lindner, T.; Somers, J. S.; Ricken, D. E.; Bradshaw, A. M. *Surf. Sci.* **1990**, *236*, 1.
(20) Yokoyama, T.; Arvanitis, D.; Lederer, T.; Tischer, M.; Tröger, L.; Baberschke, K. *Phys. Rev. B* **1993**, *48*, 15405.

(21) Lederer, T.; Arvanitis, D.; Comelli, G.; Tröger, L.; Baberschke, K. *Phys. Rev. B* **1993**, *48*, 15390.
(22) Jensen, F.; Besenbacher, F.; Lægsgaard, E.; Stensgaard, I. *Phys. Rev. B* **1990**, *42*, 9206.
(23) Rajumon, M. K.; Prabhakaran, K.; Rao, C. N. R. *Surf. Sci. Lett.* **1990**, *233*, L237.
(24) Spitzer, A.; Lüth, H. *Surf. Sci.* **1982**, *118*, 121.
(25) Zeng, H. C.; Mitchell, K. A. R. *Surf. Sci. Lett.* **1990**, *239*, L571.
(26) Fujita, T.; Okawa, Y.; Matusmoto, Y.; Tanaka, K. *Phys. Rev. B* **1996**, *54*, 2167.
(27) Ertl, G. *Surf. Sci.* **1967**, *7*, 309.
(28) Habraken, F. H. P. M.; Mesters, C. M. A. M.; Bootsma, G. A. *Surf. Sci.* **1980**, *97*, 264.
(29) Taylor, A. O.; Pritchard, J. *J. Chem. Soc., Faraday Trans.* **1990**, *86*, 2743.
(30) Muha, R. J.; Gates, S. M.; Yates, J. T., Jr.; Basu, P. *Rev. Sci. Instrum.* **1985**, *56*, 613.
(31) Andersson, S. *Surf. Sci.* **1979**, *89*, 477.
(32) Ryberg, R. *Surf. Sci.* **1982**, *114*, 627.
(33) Pritchard, J. *Surf. Sci.* **1979**, *79*, 231.
(34) Nakayama, K.; Hojo, H. *Jpn. J. Appl. Phys. Suppl.* **1974**, *2*, Part 1, 113.
(35) Brosseau, R.; Brustein, M. R.; Ellis, T. H. *Surf. Sci.* **1993**, *294*, 243.
(36) Stuve, E. M.; Jorgensen, S. W.; Madix, R. J. *Surf. Sci.* **1984**, *146*, 179.
(37) Thiel, P. A.; DePaola, R. A.; Hoffmann, F. M. *J. Chem. Phys* **1984**, *80*, 5326.
(38) Bange, K.; Grider, D. E.; Madey, T. E.; Sass, K. E. *Surf. Sci.* **1984**, *136*, 38.
(39) Sexton, B. A. *Surf. Sci.* **1980**, *94*, 435.
(40) Mitchell, G. E.; White, J. M. *Chem. Phys. Lett.* **1987**, *135*, 84.
(41) Andersson, S.; Nyberg, C.; Tengstål, C. G. *Chem. Phys. Lett.* **1984**, *104*, 305.
(42) Nyberg, C.; Tengsål, C. G. *J. Chem. Phys.* **1984**, *80*, 3463.
(43) Olle, L.; Salmerón, M.; Baró, A. M. *J. Vac. Sci. Technol. A* **1985**, *3*, 1866.
(44) Baró, A. M.; Erley, W. *J. Vac. Sci. Technol.* **1982**, *20*, 580.
(45) Crowell, J. E.; Chen, J. G.; Hercules, D. M.; Yates, J. T., Jr. *J. Chem. Phys.* **1987**, *86*, 5804.
(46) Stuve, E. M.; Madix, R. J.; Sexton, B. A. *Surf. Sci.* **1981**, *111*, 11.
(47) Fisher, G. B.; Sexton, B. A. *Phys. Rev. Lett.* **1980**, *44*, 683.
(48) Gurney, B. A.; Ho, W. *J. Chem. Phys.* **1987**, *87*, 5562.
(49) Carley, A. F.; Rassias, S.; Roberts, M. W. *Surf. Sci.* **1983**, *135*, 35.
(50) Afsin, B.; Davies, P. R.; Pashusky, A.; Roberts, M. W.; Vincent, D. *Surf. Sci.* **1993**, *284*, 109.
(51) Yoshinobu, J.; Kawai, M. *J. Chem. Phys.* **1995**, *103*, 3220.
(52) Sawabe, K.; Matsumoto, Y.; Yoshinobu, J.; Kawai, M. *J. Chem. Phys.* **1995**, *103*, 4757.
(53) Gland, J. L.; Kollin, E. B. *J. Chem. Phys.* **1983**, *78*, 963.
(54) Matsushima, T. *J. Chem. Phys.* **1990**, *93*, 1464.
(55) Matsushima, T. *Surf. Sci.* **1991**, *242*, 489.
(56) Ohno, Y.; Matsushima, T.; Shobatake, K. *Surf. Sci.* **1992**, *273*, 291.
(57) Stuve, E. M.; Madix, R. J.; Brundle, C. R. *Surf. Sci.* **1984**, *146*, 155.
(58) Matsushima, T.; Asada, H. *J. Chem. Phys.* **1986**, *85*, 1658.
(59) Matsushima, T.; Matsui, T.; Hashimoto, M. *J. Chem. Phys.* **1984**, *81*, 5151.
(60) Yang, H.; Whitten, J. L. *Surf. Sci.* **1989**, *223*, 131.
(61) Canepa, M.; Cantini, P.; Mattera, L.; Narducci, E.; Salvietti, M.; Terreni, S. *Surf. Sci.* **1995**, *322*, 271.
(62) Afsin, B.; Davies, P. R.; Pashusky, A.; Roberts, M. W. *Surf. Sci. Lett.* **1991**, *314*, L873.
(63) Kubota, J.; Kondo, J.; Domen, K.; Hirose, C. *Surf. Sci.* **1993**, *295*, 169.
(64) Barnes, C.; Pudney, P.; Guo, Q.; Bowker, M. *J. Chem. Soc., Fraday Trans.* **1990**, *86*, 2693.
(65) Madey, T. E.; Benndorf, C. *Surf. Sci.* **1985**, *152/153*, 587.
(66) Bassignana, I. C.; Wagemann, K.; Küppers, J.; Ertl, G. *Surf. Sci.* **1986**, *175*, 22.
(67) Roberts, M. W. *Surf. Sci.* **1994**, *299/300*, 769.
(68) Kulkarni, G. U.; Rao, C. N. R.; Roberts, M. W. *J. Phys. Chem.* **1995**, *99*, 3310.
(69) Carley, A. F.; Davies, P. R.; Roberts, M. W.; Shukla, N.; Song, Y.; Thomas, K. K. *Appl. Surf. Sci.* **1994**, *81*, 265.
(70) Kuk, Y.; Chua, F. M.; Silverman, P. J.; Meyer, J. A. *Phys. Rev. B* **1990**, *41*, 12393.
(71) Coulman, D.; Wintterlin, J.; Behm, R. J.; Ertl, G. *Phys. Rev. Lett.* **1990**, *64*, 1761.
(72) Jensen, F.; Besenbacher, F.; Lægsgaard, E.; Stensgaard, I. *Phys. Rev. B* **1990**, *41*, 10233.
(73) Eierdal, L.; Besenbacher, F.; Lægsgaard, E.; Stensgaard, I. *Surf. Sci.* **1994**, *312*, 31.